First-Principle Calculations of the Band Shapes of Singlet–Triplet Transitions

First Principle Calculations of the Band Shapes of Singlet-Triplet Transitions

Amalia Velardo,[†] Raffaele Borrelli,[‡] Andrea Peluso,[†] and Amedeo Capobianco[*,†]

[†]*Dipartimento di Chimica e Biologia Adolfo Zambelli, Università di Salerno, Via Giovanni Paolo II, I-84084 Fisciano (SA), Italy*

[‡]*Dipartimento di Scienze Agrarie, Forestali e Alimentari, Università di Torino, Via Leonardo da Vinci 44, I-10095 Grugliasco (TO), Italy*

E-mail: acapobianco@unisa.it

Abstract

Kubo's generating function approach has been employed for simulating from first principles the spectral band shapes of singlet-triplet transitions of some aromatic compounds, representative for their rigid structures and aromatic characters of those used in solid state opto-electronic devices. That approach yields Franck-Condon weighted densities of states in excellent agreement with experimental results, opening the way to reliable calculations of the rates of non-radiative singlet-triplet transitions, an important step for the in silico optimization of the molecular structure of dyes for solar energy conversion cells and for light emitting diodes.

Introduction

Triplet states play an important role in solid state opto-electronic devices. In organic light emitting diodes (OLED), spin statistics makes triplet excitons to be preferentially formed than singlet ones, determining to a larger extent the efficiency and the spectral features of emitted radiation.[1] In bulk heterojunctions (BHJ) photovoltaic cells, low lying triplet states could provide a potentially fast pathway for ungeminate electron-hole charge recombination, limiting the efficiency of energy conversion. Triplet excitons have been detected in BHJs under operative conditions,[2–5] but there is both experimental and theoretical evidence that charge dissociation from triplet states, even though thermally activated, is fast enough to effectively compete with relaxation of T_1 to the ground state.[4–6]

For better assessing the role triplet states play in single molecule organic devices, the rates of charge recombination and charge dissociation processes have to be evaluated.

Nonradiative transition rates can be efficiently estimated by the Fermi Golden rule (FGR):[7–11] practical experience has shown that FGR provides reliable rate constants both for very fast processes, occurring on subpicosecond timescales,[10,11] and for comparatively much slower processes. For instance, the observed temperature dependence of electron transfer (ET) from pheophytin to ubichinone in bacterial photosynthetic reaction center, a quite

slow process occurring on nanosecond timescale and involving electronic states which differ in energy by ≈ 0.9 eV, was reproduced nearly quantitatively by FGR.[12] FGR has also been successfully employed for photoinduced electron transfer processes and photoinduced electronic transitions through conical intersections.[13–16]

The FGR rate expression

$$k_{a\to b} = \frac{2\pi}{\hbar}|V_{ab}|^2 F(\Delta E, T) \tag{1}$$

depends on two quantities: the electronic coupling element, V_{ab}, and the Franck-Condon weighted density of states $F(\Delta E, T)$.

Herein, we will focus attention on the accuracy with which $F(\Delta E, T)$ can be computed from first principles for singlet triplet transitions, in the harmonic approximation. We will consider here radiative transitions for species with fused aromatic rings, as those largely employed in BHJ cells and for electron transport in organic electronics, for which experimental data are available in the literature. The calculation of $F(\Delta E, T)$ is carried out by employing Kubo's generating function (GF) approach,[12,17–23] which allows for a meaningful comparison between computed $F(\Delta E, T)$ and observed spectral band shapes, inasmuch as the GF approach makes it possible to include in computations the whole set of the molecular normal modes, taking into account both the effects due to changes of the equilibrium positions and of vibrational frequencies, as well as the effects of normal mode mixing, without posing limits to the number of modes which can be simultaneously excited and on their highest quantum number. It is shown that for radiative transitions first principle computations yield very accurate $F(\Delta E, T)$ at least in the energy region $\Delta E \approx 1 - 1.2$ eV, corresponding to the spectral bandwidth of the compounds analyzed here.

Singlet-Triplet Radiative Transitions

According to first order perturbation theory, the electric dipole transition moment for a radiative singlet triplet transition ($T_1 \leftarrow S_0$) is:[24]

$$\langle S_0|\,\gamma\,|T_1^\alpha\rangle = \sum_s \frac{\langle S_0|\,\gamma\,|S_s\rangle\,\langle S_s|\,\mathcal{H}_{\rm SO}^\alpha\,|T_1^\alpha\rangle}{E(T_1)-E(S_s)} + \sum_t \frac{\langle S_0|\,\mathcal{H}_{\rm SO}^\alpha\,|T_t^\alpha\rangle\,\langle T_t^\alpha|\,\gamma\,|T_1^\alpha\rangle}{E(S_0)-E(T_t)}, \tag{2}$$

where γ is the light polarization axis and $\mathcal{H}_{\rm SO}^\alpha$ is the α-th component of the spin orbit operator. Introducing the Born Oppenheimer approximation, neglecting non-Condon effects and the possible dependence of $\mathcal{H}_{\rm SO}^\alpha$ on the nuclear coordinates, and integrating over the electronic coordinates, the electric dipole transition element between the vibronic states $|S_0,\mathbf{v}\rangle$ and $|T_1^\alpha,\mathbf{z}\rangle$ is:

$$\langle S_0,\mathbf{v}|\,\gamma\,|T_1^\alpha,\mathbf{z}\rangle = \sum_{s,w} \frac{\mu^\gamma_{S_0,S_s}\beta^\alpha_{S_s,T_1}\langle\mathbf{v}|\mathbf{w}_s\rangle\langle\mathbf{w}_s|\mathbf{z}\rangle}{E(T_1)+\epsilon_{T_1}(\mathbf{z})-E(S_s)-\epsilon_{S_s}(\mathbf{w}_s)} + \sum_{t,w} \frac{\mu^\gamma_{T_t,T_1}\beta^\alpha_{T_t,S_0}\langle\mathbf{v}|\mathbf{w}_t\rangle\langle\mathbf{w}_t|\mathbf{z}\rangle}{E(S_0)+\epsilon_{S_0}(\mathbf{v})-E(T_t)-\epsilon_{T_t}(\mathbf{w}_t)}, \tag{3}$$

where $\mathbf{v}$, $\mathbf{z}$, $\mathbf{w}_s$, and $\mathbf{w}_t$ are multi-index vectors of the vibrational quanta of the electronic states S_0, T_1, S_s, and T_t, respectively, and ϵ their corresponding vibrational energies; $\mu^\gamma_{n,m}$ is the γ component of the transition dipole between electronic states n,m and $\beta^\alpha_{n,m}$ is the α-th component of the spin-orbit coupling.

Neglecting the vibrational contributions to the energy differences appearing at both denominators in eqn 3, and using the closure relation of the intermediate states, leads to:[25]

$$\langle S_0,\mathbf{v}|\,\gamma\,|T_1^\alpha,\mathbf{z}\rangle = \Gamma_{S_0,T_1}\langle\mathbf{v}|\mathbf{z}\rangle \tag{4}$$

where:

$$\Gamma_{S_0,T_1} = \sum_s \frac{\mu^\gamma_{S_0,S_s}\beta^\alpha_{S_s,T_1}}{E(T_1)-E(S_s)} + \sum_t \frac{\mu^\gamma_{T_t,T_1}\beta^\alpha_{T_t,S_0}}{E(S_0)-E(T_t)} \tag{5}$$

is a pure electronic factor, and $\langle\mathbf{v}|\mathbf{z}\rangle$ is the Franck-Condon integral between the vibrational

states of the singlet S_0 and the triplet T_1 states.

The assumption that vibronic energy differences can be well approximated by electronic ones is a physically well sound approximation for aromatic hydrocarbons, because the strongest spin-orbit couplings of a $\pi\pi^*$ state involve $\sigma\pi^*$ or $\pi\sigma^*$ which should be considerably higher in energy.[26,27]

For heteroaromatics the approximation could fail, because the $n\pi^*$ states are coupled to $\pi\pi^*$ states which can be close in energy. We have thus included benzophenone and carbazole in the set of investigated molecules for testing purposes.

With the assumptions discussed above, the spectral band shape for a radiative singlet-triplet transition is:[17,18]

$$I_{TS}(\nu) = \sum_v \sum_z |\Gamma_{S,T}\langle \mathbf{v}|\mathbf{z}\rangle|^2 \, \mathrm{e}^{-\beta E_{S_0,v}} \delta(E_{T,z} - E_{S_0,v} - h\nu)/Z \, ; \tag{6}$$

where Z is the partition function of the initial state. The infinite summations appearing in (6) pose computational problems which, following the seminal works of Lax and Kubo,[17,18] can be conveniently avoided by introducing the integral representation of Dirac's δ function

$$\delta(E - h\nu) = h^{-1} \int_{-\infty}^{\infty} \exp\left[\mathrm{i}\,(E - h\nu)\,\tau/\hbar\right] \mathrm{d}\tau \tag{7}$$

and writing:

$$I_{TS}(\nu) = h^{-1} \int \mathrm{d}\tau \, \mathrm{e}^{-\mathrm{i}2\pi\nu\tau} f_{TS}(\tau), \tag{8}$$

with:

$$f_{TS}(\tau) = |\Gamma_{TS}|^2 \mathrm{Tr}\, \left[\mathrm{e}^{\tau\mathcal{H}_T} \mathrm{e}^{-(\beta+\tau)\mathcal{H}_S}\right], \tag{9}$$

where $\tau = \mathrm{i}t/\hbar$, $\beta = 1/k_B T$. If the Hamiltonian operators $\mathcal{H}_S$ and $\mathcal{H}_T$ are modeled in harmonic approximation, the trace in (9) can be evaluated into a closed form.[17,19,28]

The frequency distribution function $I_{TS}(\nu)$, i.e. the spectral band shape, is then obtained by the inverse Fourier transform of the function $f_{TS}(\tau)$, c.f. Eqn 8. The approach out-

lined above provides several advantages with respect to the standard recursive calculation of Franck-Condon factors,[29–32] inasmuch as it allows to include in computations the whole manifold of vibrational states of the initial and final electronic states, and because, apart from the use of an apodization function in the fast Fourier transform,[12,19,33] no external adjustable parameters are used, thus ensuring an effective test of the performances of the electronic calculations in predicting reliable ground state and excited states geometries and vibrational frequencies.

Computational details

The computations of the ground and the first triplet states have been performed at different levels of theory, including Møller-Plesset perturbation methods for ground states and the second order algebraic diagrammatic construction for excited states [MP2/ADC(2)] and B3LYP as well as BLYP density functional theory (DFT) approaches. For naphthalene, the meta M05-2X and the range separated CAM-B3LYP hybrid functionals, both possessing a high fraction of Hartree-Fock exchange were also employed.[34–43] For carbazole, solvent effects were included in DFT computation by means of the polarizable continuum model.[44] The equilibrium geometry of the triplet T_1 state of benzophenone was also computed by using coupled cluster including single and approximate double excitations (CC2).[45] The triple zeta def2-TZVPP basis set in conjunction with the frozen core and the resolution of identity approximations has been adopted in MP2, ADC(2) and CC2 computations,[46] whereas DFT calculations have been performed using 6-31+G(d,p) basis set in conjunction with the unrestricted formalism for triplet states.[47,48] Very tight threshold values have been used in geometry optimizations together with the use of 'ultrafine' grids in all DFT computations.

Gaussian 09 and TURBOMOLE packages were used for DFT and correlated post-Hartree Fock calculations, respectively.[49,50]

Absorption spectra were computed in harmonic approximation using Kubo's generat-

ing function (GF) approach, implemented in a local development version of MolFC package.[31,33,51] Both the curvilinear and the Cartesian coordinate representation of the normal modes have been used. The former representation is useful to prevent that displacements of angular coordinates could result into unrealistic shifts of stretching coordinates upon excitation,[52–54] which should require the use of high order anharmonic potentials for its correction.[55–57]

The comparison between computed and experimental spectral band shapes has been carried out by: *i*) extracting $I_{TS}(\nu)$ from experimental spectra,[58] *ii*) normalizing both the theoretical and the experimental $I_{TS}(\nu)$'s, and *iii*) making coincident the predicted and the experimental longer or shortest wavelength peaks for absorption or emission, respectively.

Results and Discussion

We have selected a series of molecules constituted by fused aromatic rings as those used in organic electronics – specifically naphthalene, phenanthrene, 4,5-dihydropyrene, benzophenone, and carbazole (Scheme 1) – for which the $T_1 \leftarrow S_0$ (absorption) and the $T_1 \rightarrow S_0$ (emission) spectra are available in the literature, in some cases even at high resolution.[59–68]

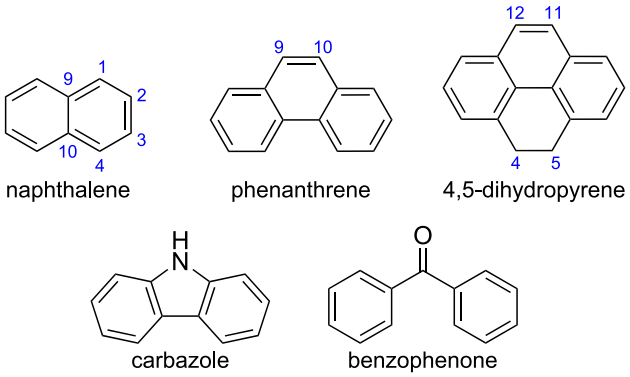

Scheme 1

Naphthalene

The experimental $T_1 \leftarrow S_0$ photoexcitation spectrum of naphthalene is characterized by an intense vibronic activity, resulting in several intense and well resolved peaks, see Figure 1, with a total bandwidth of ≈ 7000 cm^{-1}. The first peak has been assigned to the 0-0 transition;[59,68] our FC calculations confirm that assignment and, accordingly, the computed 0-0 transition energies, reported in Table 1, better agree than vertical ones with that corresponding to the observed lowest energy peak. For naphthalene MP2/ADC(2) method slightly overestimate the 0-0 transition energy, by ca 0.15 eV, whereas both B3LYP and BLYP underestimate it by 0.05 and 0.07 eV, respectively.

Table 1: Computed adiabatic ($\tilde{\nu}_{0-0}$) and vertical ($\tilde{\nu}_{\rm v}$) transition wavenumbers (cm^{-1}) for $T_1 \leftarrow S_0$ transitions.

	$\tilde{\nu}_{0-0}$			$\tilde{\nu}_{\rm v}$			
	ADC(2)	B3LYP	BLYP	ADC(2)	B3LYP	BLYP	*Exp.*[a]
naphthalene	22 285	20 560	19 914	26 391	25 048	23 554	21 186
phenanthrene	22 867	21 040	20 179	26 726	25 691	23 927	21 598
4,5-dihydropyrene	–	20 777	19 892	–	25 383	23 592	21 322
benzophenone	19 751	21 625	20 308	25 774	25 202	23 234	23 800[b]
carbazole	–	23 975	22 711	–	27 712	25 272	24 650[b]

[a]Lowest wavenumber absorption peak; [b]highest wavenumber phosphorescence peak.

Theoretical and experimental $T_1 \leftarrow S_0$ absorption spectra of naphthalene are shown in Figure 1. The theoretical spectra have been computed at $T = 77$ K with resolution of ≈ 80 cm^{-1}, slightly higher than experimental one (≈ 150 cm^{-1}),[59] causing the appearance of a few additional peaks around the most intense ones. Notwithstanding, all the theoretical approaches yield spectral band shapes in very good agreement with the observed spectrum: the five most intense peaks of the spectrum are all reproduced, with relative peak intensities comparable with the experimental ones. The large vibronic activity which characterizes the $T_1 \leftarrow S_0$ spectrum of naphthalene is due to the fact that although the point group symmetry is retained upon transition – all the theoretical methods employed here predict

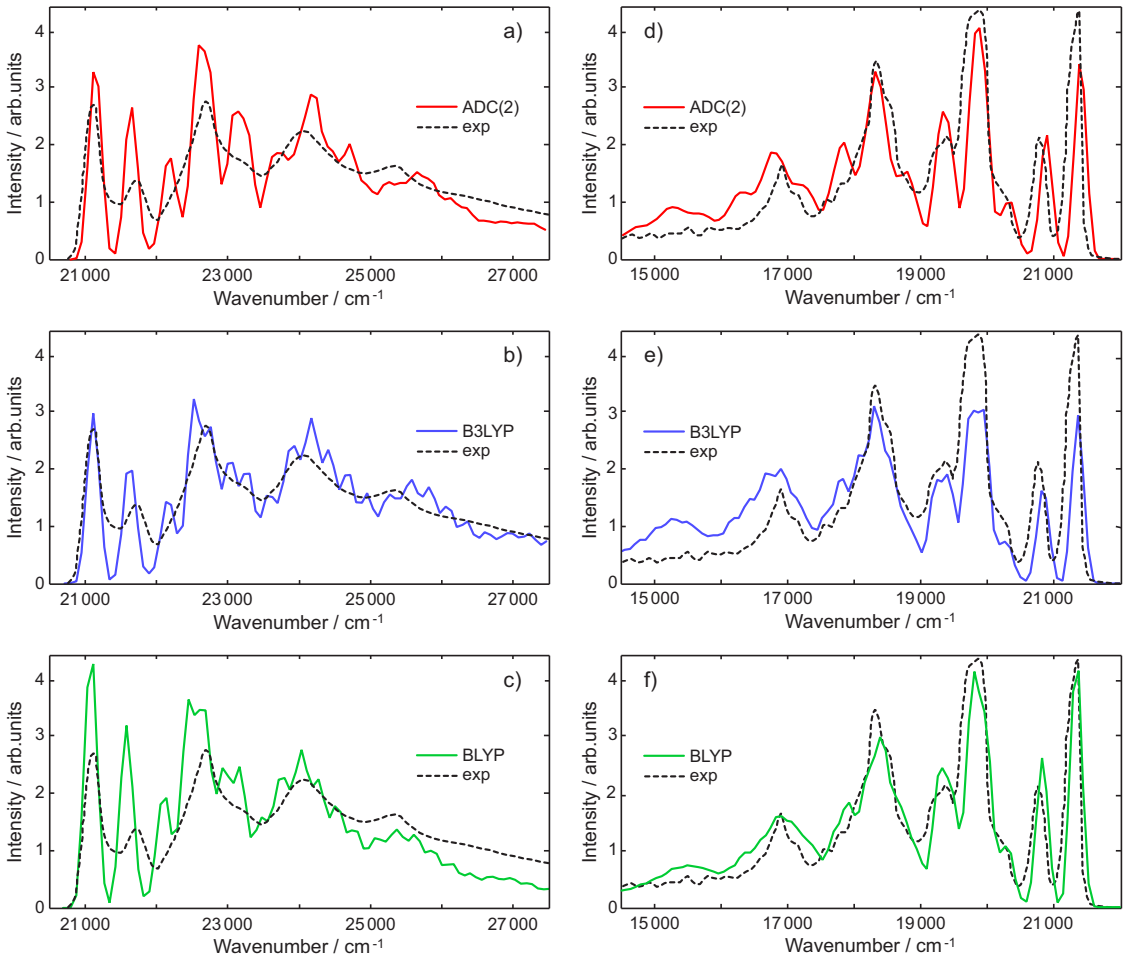

Figure 1: Theoretical and experimental (ref.s 59 and 68) $T_1 \leftarrow S_0$ (left, panels a-c) and $T_1 \rightarrow S_0$ (right, panels d-f) spectra of naphthalene at $T = 77$ K.

that naphthalene in the T_1 electronic state possesses D_{2h} symmetry – the structure of the lowest triplet state is significantly compressed with respect to the ground state one. The C2-C3 bond length is shortened (1.36 vs 1.42 Å) whereas the C1-C2 one is lengthened (1.44 vs 1.37 Å). The reported values refer to B3LYP computations, but the bond lengths predicted by the other two methods differ from B3LYP ones only on the third digit (see Table S4 in the Supporting Information).

Because the most significant geometrical changes concerns the molecular backbone, almost all totally symmetric modes, but C-H stretching ones, are displaced upon $T_1 \leftarrow S_0$ transition. The most displaced a_g modes are reported in Table 2. Computed peak wavenumbers and their vibronic assignments are reported in Table S1 of the Supporting Information,

Table 2: Wavenumbers ($\tilde{\nu}$, cm^{-1}) and equilibrium position displacements (K, adimensional units) of the most displaced normal modes of naphthalene for $T_1 \leftarrow S_0$ transition.

ADC(2)			BLYP			B3LYP		
$\tilde{\nu}_{T_1}$	$\tilde{\nu}_{S_0}$	K	$\tilde{\nu}_{T_1}$	$\tilde{\nu}_{S_0}$	K	$\tilde{\nu}_{T_1}$	$\tilde{\nu}_{S_0}$	K
500	558	1.19	492	505	1.15	505	518	1.15
1052	1143	0.61	1027	1117	0.54	1058	1172	0.61
1176	1180	0.44	1152	1154	0.37	1184	1186	0.41
1429	1485	1.26	1345	1367	1.16	1402	1410	1.37
1627	1628	1.10	1580	1607	1.07	1647	1676	1.17

together with experimental results obtained by high resolution photoexcitation spectroscopy of crystalline naphthalene.[60] The whole vibronic structure is generated by four fundamental vibrational modes falling in the T_1 state at 505, 1058, 1402, and 1647 cm^{-1} and their combination, in good agreement with experimental results.[60–62]

The experimental phosphorescence spectrum of naphthalene (Figure 1, d, e, and f panels) has been recorded in low polar medium, a mixture of methylcyc1ohexane and isopentane in 3:1 volume ratio, at $T = 77$ K.[68] As for absorption, geometries and normal modes used in the computation of the spectral band shapes were taken from gas-phase computations, which are known to yield optimal results for low polar solvents.[69]

The emission spectrum is in good approximation the mirror image of the absorption one, being characterized by five more intense peaks and a less intense one. Peak assignments are reported in Table S2 in the Supporting Information and compared with those obtained by high resolution phosphorescence spectrum.[66]

The agreement between the computed and experimental band shapes for the phosphorescence spectrum of naphthalene is very good, especially for BLYP and ADC(2), thus further testifying the reliability of the GF approach.

Phenanthrene and dihydropyrene

The singlet-triplet absorption and emission spectra of phenanthrene and diydropyrene are somewhat similar to each other and will be conveniently discussed together. For dihy-

dropyrene only DFT computations have been carried out. Predicted adiabatic and vertical transition energies are reported in Table 1. For both molecules the computed 0-0 transition energies better match with the lowest energy peaks of the $T_1 \leftarrow S_0$ excitation spectrum and indeed the first spectral peaks have been assigned to 0-0 transitions for both molecules.[70] MP2/ADC(2) slightly overestimates the 0-0 transition energy of phenanthrene by ≈ 0.16 eV, whereas both B3LYP and BLYP slightly underestimate it.

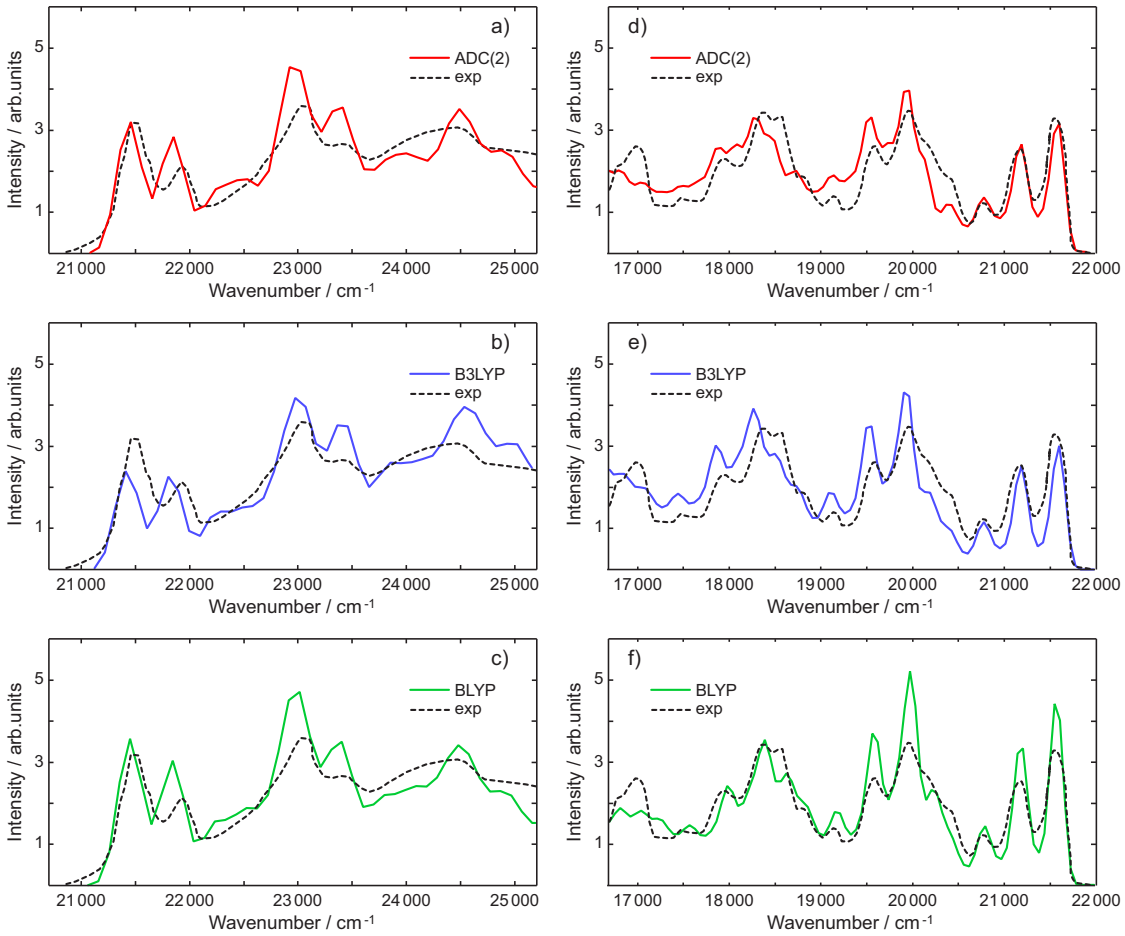

Figure 2: Theoretical and experimental (ref.s 59 and 71) $T_1 \leftarrow S_0$ (left, panels a-c, $T = 77$ K) and $T_1 \rightarrow S_0$ (right, panels d-f, $T = 90$ K) spectra of phenanthrene.

Theoretical and experimental $T_1 \leftarrow S_0$ and $T_1 \rightarrow S_0$ spectra of phenanthrene are shown in Figure 2.[59,70] Interestingly, the large vibronic activity characterizing both the absorption and emission spectra arises from only one significant geometrical change which involves the central CC bond of the central ring (the C9-C10 bond according to the standard numbering,

see Scheme 1 and Table S5 in the Supporting Information), whose length changes from 1.36 Å in S_0 to 1.46 Å in T_1, according to all the computational approaches employed here. The C_{2v} symmetry is retained in the triplet state. The most displaced normal modes of phenanthrene upon $T_1 \leftarrow S_0$ transition are reported in Table 3. Although several modes are predicted to change their equilibrium positions, spectral peaks of both absorption and emission spectra can all be assigned to the two most displaced modes, the first one falling at low frequency (≈ 400 cm^{-1}), see table 3, corresponding to a breathing mode of the whole molecule, the other at high frequency (1550-1600 cm^{-1}), corresponding to a collective CC symmetric stretching. Peaks assignments of the phosphorescence spectrum are reported in Table S3 of the Supporting Information and compared with the available experimental data.[72]

Table 3: Wavenumbers ($\tilde{\nu}$, cm^{-1}) and equilibrium position displacements (K, adimensional units) of the most displaced normal modes of phenanthrene for $T_1 \leftarrow S_0$ transition.

ADC(2)			BLYP			B3LYP		
$\tilde{\nu}_{T_1}$	$\tilde{\nu}_{S_0}$	K	$\tilde{\nu}_{T_1}$	$\tilde{\nu}_{S_0}$	K	$\tilde{\nu}_{T_1}$	$\tilde{\nu}_{S_0}$	K
397	437	1.25	391	399	1.25	401	411	1.32
1009	1057	0.57	996	1030	0.44	1012	1063	0.60
1067	1110	0.50	1038	1082	0.54	1069	1116	0.42
1434	1472	0.82	1383	1410	0.15	1425	1458	0.13
1512	1537	0.55	1443	1488	0.32	1500	1540	0.33
1575	1653	0.93	1506	1585	0.29	1570	1649	0.38
1616	1662	0.66	1562	1597	1.26	1615	1667	1.34

Predicted spectral band shapes of the $T_1 \leftarrow S_0$ and $T_1 \rightarrow S_0$ spectra of 4,5-dihydropyrene (Figure 3) are very similar to those of phenanthrene (Figure 2), inasmuch as the molecule undergoes the same large elongation of the C11-C12 double bond of the central ring as predicted for phenanthrene, see Scheme 1 and Table S6 of the Supporting Information. Both B3LYP and BLYP functionals predict that S_0 and T_1 states possess C_2 point symmetry.

The experimental excitation spectrum has been truncated at 25 800 cm^{-1}, because at higher wavenumbers the $T_2 \leftarrow S_0$ transition overlaps with the $T_1 \leftarrow S_0$ one.[59] The signif-

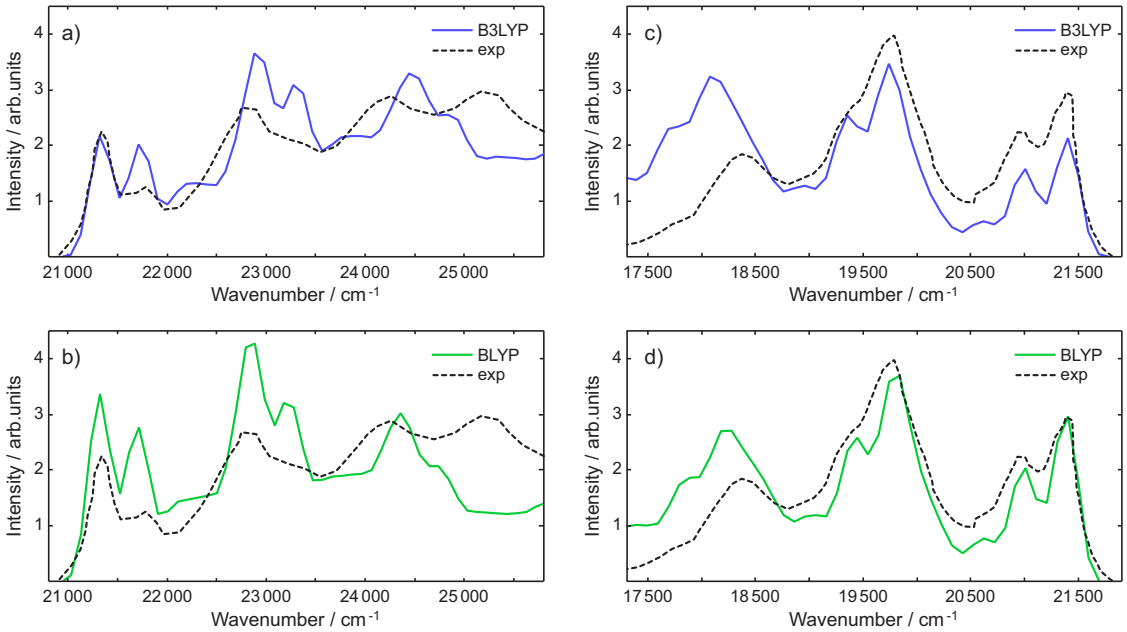

Figure 3: Theoretical and experimental (59) spectra of $T_1 \leftarrow S_0$ (left panels) and $T_1 \rightarrow S_0$ (right panels) transitions of 4-5,dihydropyrene at 77 K.

icant discrepancies between theoretical and the experimental band shapes in the region of higher wavenumbers, much larger than those pertaining to naphthalene and phenanthrene, are possibly attributable to the presence of that additional absorption; indeed the agreement between computed and observed spectra is much more satisfying for the phosphorescence spectrum than for the absorption one, testifying about the reliability of the predicted geometrical distortions between S_0 and T_1.

Benzophenone

The phosphorescence spectrum of benzophenone recorded in low-polarity environment, i.e. glassy EPA (diethyl ether, isopentane, and ethanol, 5:5:2 volume ratio) at 77 K exhibits an intense vibronic progression, characterized by five peaks spaced by ≈ 1800 cm^{-1},[73,74] which indicates that the $T_1 \rightarrow S_0$ transition is accompanied by a significant change of the CO bond distance.

The experimental and predicted spectra are shown in Figure 4. Both BLYP and in

particular B3LYP methods yield phosphorescence band shapes in excellent agreement with the experimental results, whereas the MP2/ADC(2) approach gives a very broad spectrum extending over 30 000 cm^{-1}, part of which (the shortest wavelength region) has been reported in Figure 4, for the whole spectrum see Figure S1 in the Supporting Information. The analysis of the computed geometrical parameters of S_0 and T_1, see Table S7 in the Supporting Information, clearly shows that the failure of MP2/ADC(2) approach is due to its high overestimation of the CO bond length in the T_1 states, which is predicted to be 1.413 Å, a value corresponding to the length of a single CO bond, whereas BLYP and B3LYP yield 1.32 and 1.33 Å, respectively. The other important geometrical changes concern the two CC bond lengths at the carbonyl group, which are shortened in the T_1 state, and the ∠CCC valence bond angle at the carbonyl carbon, which increases in the T_1 state. MP2/ADC(2) highly overestimates all those geometrical changes, in line with the predicted reorganization energy, amounting to ca 6000 cm^{-1}, significantly higher than that obtained by DFT computations ($\approx$ 4000 cm^{-1}, see Table 1). Finding out the reasons of that failure is out of the scopes of this paper; occasional overestimations of double-bond lengths, in particular those involving oxygen atoms, have been previously found for the CC2 approach, to which ADC(2) is closely related. Indeed in our case also CC2 overestimates the C–O bond length of the triplet state, giving 1.408 Å. The interested reader can consult references 75 and 76 which, although not dealing with the specific case of triplets, discuss how the main approximation of the theoretical approach could affect equilibrium geometries.

The most displaced normal modes of benzophenone are reported in Table 4. Both S_0 and T_1 are predicted to possess C_2 symmetry. Apart a few low frequency modes, the most displaced mode is the CO symmetric stretching. In the T_1 state that mode is predicted to also undergo a significant shift in frequency, which changes from ca 1700 cm^{-1} in S_0 to ca 1250 cm^{-1}, according to DFT methods, and 950 cm^{-1}, according to ADC(2). The symmetric stretching involving the carbonyl carbon atom are also displaced, but to a lower extent, without causing observable progressions in the phosphorescence spectrum, which is

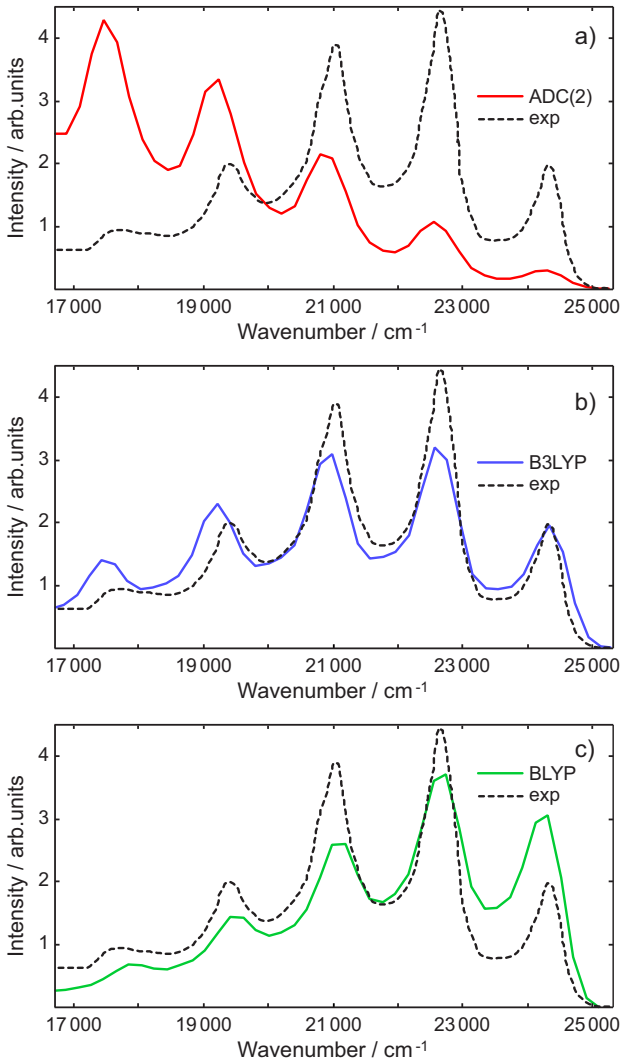

Figure 4: Theoretical and experimental (ref 73) spectra of $T_1 \rightarrow S_0$ transition of benzophenone at 77 K.

completely dominated by the CO stretching progression.

Table 4: Wavenumbers ($\tilde{\nu}$, cm^{-1}) and equilibrium position displacements (K, adimensional units) of the most displaced normal modes of benzophenone for $T_1 \rightarrow S_0$ transition.

B3LYP			BLYP			ADC(2)		
$\tilde{\nu}_{S_0}$	$\tilde{\nu}_{T_1}$	K	$\tilde{\nu}_{S_0}$	$\tilde{\nu}_{T_1}$	K	$\tilde{\nu}_{S_0}$	$\tilde{\nu}_{T_1}$	K
63	68	2.30	61	65	2.18	65	67	3.92
92	90	0.75	88	84	1.01	1620	1597	0.60
1645	1612	0.56	1575	1537	0.73	1638	1623	0.55
1718	1275	1.82	1623	1255	1.21	1698	950	3.36

Carbazole

Carbazole is an important dye; poly(N-vinylcarbazole) has been among the first reported electroluminescent polymers and, although the interest in that system has decreased upon the development of much more efficient phosphorescent molecules, it is still attracting interest as hosts for triplet emitters in OLED.[77]

The phosphorescence spectrum of carbazole in butyronitrile glass is reported in Figure 5,[78] together with the spectral band shapes obtained by B3LYP and BLYP computations. MP2/ADC(2) has not been used in that case because molecular geometry optimizations with ADC(2) including solvation are not yet available in TURBOMOLE. For both functionals, geometry optimizations of the T_1 state yield a C_{2v} structure with one imaginary frequency. The optimization was then refined by slightly distorting the C_{2v} geometries along the imaginary frequency mode and led to a more stable planar structure (ca 5 kcal/mol) loosely belonging to C_{2v} point group, which has been used in spectral shape computations reported in Figure 5.

Both functionals yield very satisfying results: the band shapes are reliably reproduced over the whole spectral range, which extends from 25 000 to $\approx$ 16 000 cm^{-1}, indicating that the molecule undergoes significant geometry reorganization in going from the ground state to the first excited state. The most relevant geometrical parameters of S_0 and T_1 are reported

in Table S8 of the Supporting Information. The relevant geometrical variations in the triplet state mostly concern the CC bonds of the pyrrole ring: the formally single CC bond is significantly shortened, from 1.46 Å to 1.39 and 1.41 Å, according to B3LYP and BLYP, respectively. The other two CC bonds of the pyrrole ring are elongated by ca 0.05 Å. Those CC bond variations reflect in a large number of normal modes whose equilibrium positions are displaced upon $T_1 \rightarrow S_0$ transition; the largest displacements are reported in Table 5.

Table 5: Wavenumbers ($\tilde{\nu}$, cm^{-1}) and equilibrium position displacements (K, adimensional units) of the most displaced normal modes of carbazole for $T_1 \rightarrow S_0$ transition.

BLYP			B3LYP		
$\tilde{\nu}_{T_1}$	$\tilde{\nu}_{S_0}$	K	$\tilde{\nu}_{T_1}$	$\tilde{\nu}_{S_0}$	K
546	496	0.54	560	508	0.47
730	667	0.46	754	692	0.72
998	948	0.42	886	778	0.50
1264	1257	0.62	1309	1264	0.71
1389	1365	0.46	1336	1292	0.55
1554	1494	0.59	1620	1580	0.53
1596	1536	0.80	1664	1622	1.21

The most displaced modes are two collective total symmetric stretching and bending modes falling at $\approx$ 1600 and 1200 cm^{-1}; the former is responsible of the two most intense peaks of the phosphorescence spectrum falling at ca 23 000 and 21 300 cm^{-1}, whereas the latter causes the less intense peak at $\approx$ 24 000 cm^{-1}. All other peaks are combination bands of these two modes with the other less displaced modes reported in Table 5.

Conclusion

The optimization of technological devices for a sustainable development, solar energy conversion and low cost light emitting diodes, requires the tailoring of several molecular properties to achieve their optimal efficiencies. That is a difficult task which has to be carried out on different lines, concerning not only the energy positions of molecular levels but also the rates of radiationless processes which could take place in devices, and the fine matching of spec-

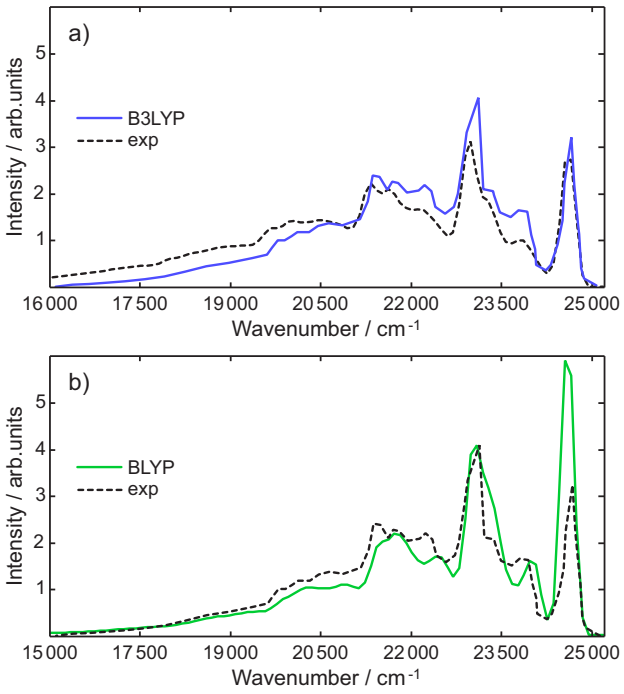

Figure 5: Theoretical and experimental (ref 78) $T_1 \rightarrow S_0$ spectra of carbazole at 77 K.

tral bands, which control energy transfer processes.[6,69,77] Herein we have shown that modern computational procedures allow for simulating spectral band shapes of singlet-triplet transitions, yielding very reliable Franck-Condon weighted densities of states in a wide spectral region, up to 1-1.2 eV. The employment of Kubo's generating function approach is crucial in that task, inasmuch as it allows to include in calculations all the molecular normal modes of vibration and all the effects which affect the Franck-Condon density of states, i.e. equilibrium position displacements, normal mode mixing, and vibrational frequency changes. The approach is therefore also very useful for testing the ability of first principle calculations in predicting those quantities for triplet states, for which spectral band shapes are often the only experimental data available in the literature.

For the systems analyzed in this work, all the tested electronic methodologies provide reliable band shapes for singlet-triplet transitions. With the exception of benzophenone (see Figure 4), MP2/ADC(2) outperforms DFT, but only to a small extent, not fully commensurate with its higher computational cost. The pure BLYP functional, the less demanding

among the used methods, gives band-shapes in very good agreement with observed spectra, but slightly underestimates transition energies. Limited to naphthalene, we have also tested the M05-2X and CAM-B3LYP high-exchange functionals, which furnished very good ground and excited state equilibrium geometries for aromatic dipolar dyes.[69,79,80] Figure S2 in the Supporting Information shows that both M05-2X and CAM-B3LYP behave worse than BLYP and B3LYP functionals, predicting spectral bandwidths larger than their experimental counterparts both for $T_1 \leftarrow S_0$ and $T_1 \rightarrow S_0$ transitions, possibly due to anharmonic effects.[69] Based on the present data, B3LYP appears to be a good compromise between accuracy and computational cost, as it gives good band shapes and also well reproduces the observed 0-0 transition energies.

Acknowledgement

The financial supports of PON2007-2014 (Relight project) and of the University of Salerno are gratefully acknowledged. A. C. acknowledges the CINECA award HP10CYW18T under the ISCRA initiative, for the availability of high performance computing resources.

Supporting Information Available

Assignments of vibronic peaks (Tables S1-S3); displaced internal coordinates for S_0 and T_1 states (Tables S4-S8); complete MP2/ADC(2) phosphorescence spectrum of benzophenone (Figure S1) Absorption and phosphorescence spectra of naphthalene predicted by CAM-B3LYP and M05-2X functionals (Figure S2). This material is available free of charge via the Internet at `http://pubs.acs.org/`.

References

(1) Baldo, M. A.; Thompson, M. E.; Forrest, S. R. High-Efficiency Fluorescent Organic Light-Emitting Devices Using a Phosphorescent Sensitizer. *Nature* **1999**, *403*, 750–753.

(2) Veldman, D.; Meskers, S. C. J.; Janssen, R. A. J. The Energy of Charge-Transfer States in Electron Donor-Acceptor Blends: Insight into the Energy Losses in Organic Solar Cells. *Adv. Funct. Mater.* **2009**, *19*, 1939–1948.

(3) Piliego, C.; Loi, M. A. Charge Transfer State in Highly Efficient Polymer-Fullerene Bulk Heterojunction Solar Cells. *J. Mater. Chem.* **2012**, *22*, 4141–4150.

(4) Rao, A.; Chow, P. C. Y.; Gélinas, S.; Schlenker, C. W.; Li, C.-Z.; Yip, H.-L.; Jen, A. K.-Y.; Ginger, D. S.; Friend, R. H. The Role of Spin in the Kinetic Control of Recombination in Organic Photovoltaics. *Nature* **2013**, *500*, 435–439.

(5) Chow, P. C. Y.; Albert-Seifried, S.; Gélinas, S.; Friend, R. H. Nanosecond Intersystem Crossing Times in Fullerene Acceptors: Implications for Organic Photovoltaic Diodes. *Adv. Mater.* **2014**, *26*, 4851–4854.

(6) Velardo, A.; Borrelli, R.; Capobianco, A.; La Rocca, M. V.; Peluso, A. First Principle Analysis of Charge Dissociation and Charge Recombination Processes in Organic Solar Cells. *J. Phys. Chem. C* **2015**, *119*, 18870–18876.

(7) Peng, Q.; Yi, Y.; Shuai, Z.; Shao, J. Excited State Radiationless Decay Process with Duschinsky Rotation Effect: Formalism and Implementation. *J. Chem. Phys.* **2007**, *126*, 114302–8.

(8) Peng, Q.; Yi, Y.; Shuai, Z.; Shao, J. Toward Quantitative Prediction of Molecular Fluorescence Quantum Efficiency: Role of Duschinsky Rotation. *J. Am. Chem. Soc.* **2007**, *129*, 9333–9339.

(9) Borrelli, R.; Peluso, A. Elementary Electron Transfer Reactions: from Basic Concepts to Recent Computational Advances. *WIREs: Comput. Mol. Sci.* **2013**, *3*, 542–559.

(10) Borrelli, R.; Capobianco, A.; Peluso, A. Hole Hopping Rates in Single Strand Oligonucleotides. *Chem. Phys.* **2014**, *440*, 25–30.

(11) Borrelli, R.; Capobianco, A.; Landi, A.; Peluso, A. Vibronic Couplings and Coherent Electron Transfer in Bridged Systems. *Phys. Chem. Chem. Phys.* **2015**, *17*, 30937–30945.

(12) Borrelli, R.; Peluso, A. The Temperature Dependence of Radiationless Transition Rates from Ab Initio Computations. *Phys. Chem. Chem. Phys.* **2011**, *13*, 4420–4426.

(13) Lee, M. H.; Dunietz, B. D.; Geva, E. Calculation from First Principles of Intramolecular Golden-Rule Rate Constants for Photo-Induced Electron Transfer in Molecular Donor-Acceptor Systems. *J. Phys. Chem. C* **2013**, *117*, 23391–23401.

(14) Lee, M. H.; Geva, E.; Dunietz, B. D. Calculation from First-Principles of Golden Rule Rate Constants for Photoinduced Subphthalocyanine/Fullerene Interfacial Charge Transfer and Recombination in Organic Photovoltaic Cells. *J. Phys. Chem. C* **2014**, *118*, 9780–9789.

(15) Izmaylov, A. F.; Mendive-Tapia, D.; Bearpark, M. J.; Robb, M. A.; Tully, J. C.; Frisch, M. J. Nonequilibrium Fermi Golden Rule for Electronic Transitions through Conical Intersections. *J. Chem. Phys.* **2011**, *135*, 234106.

(16) Endicott, J. S.; Joubert-Doriol, L.; Izmaylov, A. F. A Perturbative Formalism for Electronic Transitions through Conical Intersections in a Fully Quadratic Vibronic Model. *J. Chem. Phys.* **2014**, *141*, 034104.

(17) Kubo, R.; Toyozawa, Y. Application of the Method of Generating Function to Radiative and Non-Radiative Transitions of a Trapped Electron in a Crystal. *Prog. Theor. Phys.* **1955**, *13*, 160–182.

(18) Lax, M. The Franck-Condon Principle and Its Application to Crystals. *J. Chem. Phys.* **1952**, *20*, 1752–1760.

(19) Borrelli, R.; Capobianco, A.; Peluso, A. Generating Function Approach to the Calculation of Spectral Band Shapes of Free-Base Chlorin Including Duschinsky and Herzberg-Teller Effects. *J. Phys. Chem. A* **2012**, *116*, 9934–9940.

(20) Baiardi, A.; Bloimo, J.; Barone, V. General Time Dependent Approach to Vibronic Spectroscopy Including Franck-Condon, Herzberg-Teller, and Duschinsky Effects. *J. Chem. Theory Comput.* **2013**, *9*, 4097–4115.

(21) Huh, J.; Berger, R. Application of Time-Independent Cumulant Expansion to Calculation of Franck-Condon Profiles for Large Molecular Systems. *Faraday Discuss.* **2011**, *150*, 363–373.

(22) Avila Ferrer, F. J.; Cerezo, J.; Stendardo, E.; Improta, R.; Santoro, F. Insights for an Accurate Comparison of Computational Data to Experimental Absorption and Emission Spectra: Beyond the Vertical Transition Approximation. *J. Chem. Theory Comput.* **2013**, *9*, 2072–2082.

(23) Huh, J.; Berger, R. Coherent State-Based Generating Function Approach for Franck-Condon Transitions and Beyond. *JPCS* **2012**, *380*, 012019.

(24) Minaev, B.; Ågren, H. The Interpretation of the Wulf Absorption Band of Ozone. *Chem. Phys. Lett.* **1994**, *217*, 531–538.

(25) Kresin, V. Z.; Lester, W. A. On the Mechanism of Singlet-Triplet Transitions. *Chem. Phys. Lett.* **1987**, *138*, 59–64.

(26) Breiland, W. G.; Harris, C. B. Breakdown of the Born-Oppenheimer Approximation in Radiative Transitions. *Chem. Phys. Lett.* **1973**, *18*, 309–314.

(27) Turro, N. J. *Modern Molecular Photochemistry*; University Science Books, 1991.

(28) Husimi, K. Some Formal Properties of the Density Matrix. *Proc. Phys.-Math. Soc. Jpn.* **1940**, *22*, 264–314.

(29) Doktorov, E. V.; Malkin, I. A.; Man'ko, V. I. Dynamical Symmetry of Vibronic Transitions in Polyatomic Molecules and the Franck-Condon Principle. *J. Mol. Spectrosc.* **1977**, *64*, 302–326.

(30) Peluso, A.; Santoro, F.; Del Re, G. Vibronic Coupling in Electronic Transitions with Significant Duschinsky Effect. *Int. J. Quant. Chem.* **1997**, *63*, 233–244.

(31) Borrelli, R.; Peluso, A. Dynamics of Radiationless Transitions in Large Molecular Systems: A Franck-Condon Based Method Accounting for Displacements and Rotations of All the Normal Coordinates. *J. Chem. Phys.* **2003**, *119*, 8437–8448.

(32) Santoro, F.; Lami, A.; Improta, R.; Bloimo, J.; Barone, V. Effective Method for the Computation of Optical Spectra of large Molecules at Finite Temperature Including the Duschinsky and Herzberg-Teller Effect: The Band of Porphyrin as a Case Study. *J. Chem. Phys.* **2008**, *128*, 224311.

(33) Borrelli, R.; Capobianco, A.; Peluso, A. Franck-Condon Factors: Computational Approaches and Recent Developments. *Can. J. Chem.* **2013**, *91*, 495–504.

(34) Schirmer, J. Beyond the Random-phase Approximation: A New Approximation Scheme for the Polarization Propagator. *Phys. Rev. A* **1982**, *26*, 2395–2416.

(35) Trofimov, A. B.; Schirmer, J. An Efficient Polarization Propagator Approach to Valence Electron Excitation Spectra. *J. Phys. B* **1995**, *28*, 2299–2324.

(36) Hättig, C. Structure Optimizations for Excited States with Correlated Second-Order Methods: CC2 and ADC(2). *Phys. Chem. Chem. Phys.* **2002**, *50*, 37–60.

(37) Hättig, C.; Hald, K. Implementation of RI-CC2 Triplet Excitation Energies with an Application to Trans-Azobenzene. *Phys. Chem. Chem. Phys.* **2002**, *4*, 2111–2118.

(38) Hättig, C.; Köhn, A.; Hald, K. First-Order Properties for Triplet Excited States in the Approximated Coupled Cluster Model CC2 Using an Explicitly Spin Coupled Basis. *J. Chem. Phys.* **2002**, *116*, 5401–5410.

(39) Hättig, C.; Weigend, F. CC2 Excitation Energy Calculations on Large Molecules Using the Resolution of the Identity Approximation. *J. Chem. Phys.* **2000**, *113*, 5154–5161.

(40) Becke, A. D. Density-Functional Thermochemistry. III. The Role of Exact Exchange. *J. Chem. Phys.* **1993**, *98*, 5648–5652.

(41) Stephens, P. J.; Devlin, F. J.; Chabalowski, C. F.; Frisch, M. J. Ab Initio Calculation of Vibrational Absorption and Circular Dichroism Spectra Using Density Functional Force Fields. *J. Phys. Chem.* **1994**, *98*, 11623–11627.

(42) Zhao, Y.; Schultz, N. E.; Truhlar, D. G. Design of Density Functionals by Combining the Method of Constraint Satisfaction with Parametrization for Thermochemistry, Thermochemical Kinetics, and Noncovalent Interactions. *J. Chem. Theory Comput.* **2006**, *2*, 364–382.

(43) Yanai, T.; Tew, D. P.; Handy, N. C. A New Hybrid Exchange-Correlation Functional Using the Coulomb-Attenuating Method (CAM-B3LYP). *Chem. Phys. Lett.* **2004**, *393*, 51–57.

(44) Miertuš, S.; Scrocco, E.; Tomasi, J. Electrostatic Interaction of a Solute with a Continuum. A Direct Utilization of Ab Initio Molecular Potentials for the Prevision of Solvent Effects. *Chem. Phys.* **1981**, *55*, 117–129.

(45) Christiansen, O.; Koch, H.; Jørgensen, P. The Second-Order Approximate Coupled Cluster Singles and Doubles Model CC2. *Chem. Phys. Lett.* **1995**, *243*, 409–418.

(46) Häser, M.; Patzelt, H.; R. Ahlrichs, R. RI-MP2: Optimized Auxiliary Basis Sets and Demonstration of Efficiency. *Chem. Phys. Lett.* **1998**, *294*, 143.

(47) Hehre, W. J.; Ditchfield, R.; Pople, J. A. Self-Consistent Molecular Orbital Methods. XII. Further Extensions of Gaussian-Type Basis Sets for Use in Molecular Orbital Studies of Organic Molecules. *J. Chem. Phys.* **1972**, *56*, 2257–2261.

(48) Clark, T.; Chandrasekhar, J.; Spitznagel, G. W.; Schleyer, P. v. R. Efficient Diffuse Function-Augmented Basis-Sets for Anion Calculations. 3. The 3-21+G Basis Set for 1st-Row Elements, Li-F. *J. Comp. Chem.* **1983**, *4*, 294–301.

(49) Frisch, M. J.; Trucks, G. W.; Schlegel, H. B.; *al*, E.-T. Gaussian 09 Revision D.01. Gaussian Inc. Wallingford CT 2009.

(50) TURBOMOLE V6.3.1 2011, a development of University of Karlsruhe and Forschungszentrum Karlsruhe GmbH, 1989-2007, TURBOMOLE GmbH, since 2007; available from `http://www.turbomole.com`.

(51) Borrelli, R.; Peluso, A. MolFC: A program for Franck-Condon integrals calculation. Package available online at `http://www.theochem.unisa.it`.

(52) Borrelli, R.; Peluso, A. The Vibrational Progressions of the N ← V Electronic Transition of Ethylene. A Test Case for the Computation of Franck-Condon Factors of Highly Flexible Photoexcited Molecules. *J. Chem. Phys.* **2006**, *125*, 194308–8.

(53) Borrelli, R.; Peluso, A. Erratum: "The Vibrational Progressions of the N ← V Electronic Transition of Ethylene: A Test Case for the Computation of Franck-Condon Factors of Highly Flexible Photoexcited Molecules". *J. Chem. Phys.* **2013**, *139*, 159902–1.

(54) Capobianco, A.; Borrelli, R.; Noce, C.; Peluso, A. Franck-Condon Factors in Curvilinear Coordinates: The Photoelectron Spectrum of Ammonia. *Theor. Chem. Acc.* **2012**, *131*, 1181.

(55) Peluso, A.; Borrelli, R.; Capobianco, A. Photoelectron Spectrum of Ammonia, a Test Case for the Calculation of Franck–Condon Factors in Molecules Undergoing Large Geometrical Displacements upon Photoionization. *J. Phys. Chem. A* **2009**, *113*, 14831–14837.

(56) Peluso, A.; Borrelli, R.; Capobianco, A. Correction to "Photoelectron Spectrum of Ammonia, a Test Case for the Calculation of Franck-Condon Factors in Molecules Undergoing Large Geometrical Displacements upon Photoionization". *J. Phys. Chem. A* **2013**, *117*, 10985–10985.

(57) Hoy, A. R.; Mills, I. M.; Strey, G. Anharmonic Force Constant Calculations. *Mol. Phys.* **1972**, *24*, 1265–1290.

(58) Parson, W. W. *Modern Optical Spectroscopy with Exercises and Examples from Biophysics and Biochemistry*; Springer-Verlag, Berlin Heidelberg, 2007.

(59) Marchetti, A. P.; Kearns, D. R. Investigation of Singlet-Triplet Transitions by the Phosphorescence Excitation Method. IV. The Singlet-Triplet Absorption Spectra of Aromatic Hydrocarbons. *J. Am. Chem. Soc.* **1966**, *89*, 768–777.

(60) Castro, G.; Robinson, W. Singlet- Triplet Absorption of Crystalline Naphtalene by High-Resolution Photoexcitation Spectroscopy. *J. Chem. Phys.* **1969**, *50*, 1159–1164.

(61) Abramson, E.; Avakian, P. Singlet-Triplet Exciton Absorption Spectra in Naphthalene and Pyrene Crystals. *J. Chem. Phys.* **1965**, *43*, 821–823.

(62) Ferguson, J.; Iredale, T.; Taylor, J. A. The Phosphorescence Spectra of Naphthalene and Some Simple Derivatives. *J. Chem. Soc.* **1954**, 3160–3165.

(63) Hanson, M. D. Phosphorescence Spectrum, Vibronic Analysis, and Lattice Frequencies of the Naphthalene Molecule in a Deuteronaphthalene Crystal. *J. Chem. Phys.* **1969**, *51*, 5063–5069.

(64) Priestley, E. B.; Haug, A. Phosphorescence Spectrum of Pure Crystalline Naphthalene. *J. Chem. Phys.* **1968**, *49*, 622–629.

(65) Pavlopoulos, T. G. Vibrational Assignment of Naphthalene Phosphorescence. *Mol. Phys.* **1968**, *14*, 87–92.

(66) McGlynn, S. P.; Reynolds, M. J.; Daigre, G. W.; Christodoy, N. D. The External Heavy-Atom Spin-Orbital Coupling Effect. III. Phosphorescence Spectra and Lifetimes of Externally Perturbed Naphthalenes. *J. Phys. Chem.* **1962**, *66*, 2499–2505.

(67) Gilbert, N.; Lewis, G.; Kasha, M. Phosphorescence and the Triplet State. *J. Chem. Phys.* **1944**, *66*, 2100–2116.

(68) Yanagidate, M.; Takayama, K.; Takeuchi, M.; Shizuka, H. Molecular Conformation Effects on the Relaxation Processes in the Excited State of Naphthalenophanes. *J. Phys. Chem.* **1993**, *97*, 8881–8888.

(69) Capobianco, A.; Borrelli, R.; Landi, A.; Velardo, A.; Peluso, A. Absorption Band Shapes of a Push-Pull Dye Approaching the Cyanine Limit: A Challenging Case for First Principle Calculations. *J. Phys. Chem. A* **2016**, *120*, 5581–5589.

(70) Arnold, S.; Whitten, B. Triplet Excitation Spectrum of Phenanthrene Crystals, Molecular Crystals and Liquid Crystals. *Mol. Cryst. Liq. Cryst.* **1972**, *18*, 83–86.

(71) Kanda, Y.; Shimada, R. The Triplet-Singlet Emission Spectra of Phenanthrene and Related Compounds in EPA and in Petroleum Ether at 90 K. *Spectrochimica Acta* **1959**, *15*, 211–224.

(72) Azumi, T.; McGlynn, S. P. Polarization of the Luminescence of Phenanthrene. *J. Chem. Phys.* **1962**, *37*, 2413.

(73) Simpson, J. D.; Offen, H. W. Pressure Dependence of Benzophenone Phosphorescence. *J. Chem. Phys.* **1970**, *52*, 1467.

(74) Simpson, J. D.; Offen, H. W. Phosphorescence of Benzophenone, Benzophenone-d10, and Decafluorobenzophenone in Rigid Glasses and Crystals under Pressure. *J. Chem. Phys.* **1971**, *55*, 4832.

(75) Hättig, C. Geometry Optimizations with the Coupled-Cluster Model CC2 Using the Resolution-Of-The-Identity Approximation. *J. Chem. Phys.* **2003**, *118*, 7751–7761.

(76) Wang, Z.; Wang, F. Analysis of a Failure of the CC2 Coupled-Cluster Method for Bond Lengths of SnO and PbO. *Theor. Chem. Acc.* **2014**, *133*, 1579.

(77) Marsal, P.; Avilov, I.; da Silva Filho, D. A.; Brédas, J. L.; Beljonne, D. Molecular Hosts for Triplet Emission in Light Emitting Diodes: A Quantum-Chemical Study. *Chem. Phys. Lett.* **2004**, *392*, 521–528.

(78) Baschieri, A.; Sambri, L.; Gualandi, I.; Tonelli, D.; Monti, F.; Degli Esposti, A.; Armaroli, N. Carbazole-Terpyridine Donor-acceptor Luminophores. *RSC Adv.* **2013**, *3*, 6507–6517.

(79) Capobianco, A.; Centore, R.; Noce, C.; Peluso, A. Molecular Hyperpolarizabilities of Push-Pull Chromophores: A Comparison between Theoretical and Experimental Results. *Chem. Phys.* **2013**, *411*, 11–16.

(80) Capobianco, A.; Esposito, A.; Caruso, T.; Borbone, F.; Carella, A.; Centore, R.; Peluso, A. Tuning Wavefunction Mixing in Push–Pull Molecules: From Neutral to Zwitterionic Compounds. *Eur. J. Org. Chem.* **2012**, 2980–2989.

Graphical TOC Entry